# Simulated trends in land surface sensible heat flux on the Tibetan Plateau and the possible causes

**Shuzhou Wang** ( wangsz@nuist.edu.cn )
Nanjing University of Information Science and Technology https://orcid.org/0000-0003-3267-0124
**Liu Yuxin**
**Yaoming Ma**

**Research Article**

**Keywords:** Tibetan Plateau, land surface model, sensible heat flux, trend

**Posted Date:** February 8th, 2022

**DOI:** https://doi.org/10.21203/rs.3.rs-1331058/v1

# Abstract

Characteristics of spatial distribution and variation of surface sensible heat (SH) flux on the Tibetan Plateau (TP) were studied using the simulation results from the Noah-MP land surface model for the period of 1985-2015. The inter-annual variations and possible causes were also analyzed. It is found that, the western and central TP witnessed much larger 31-yr mean SH fluxes than the eastern TP. Meanwhile, the inter-annual variations of SH fluxes on the central and western TP were larger than that on the eastern TP. All the regions showed a decreasing trend in SH flux from mid-1980s, but an increasing trend since the beginning of the 21st century. However, the eastern TP got the increasing trend later than the western and central TP. On the whole, the increasing trend began from about 2002. The western and central TP had larger values of $Ts–Ta$ (difference between ground and air temperature) than the eastern TP. Overall, the trends of mean $Ts–Ta$ and SH flux were similar to each other. The changes of mean $Ts–Ta$ were the main causes of the decreasing and increasing trends in SH flux on the TP. Meanwhile, the changes of wind speed contributed a lot to the trends of SH flux before 1998. There were no clear trends in heat transfer coefficient $C_H$.


# 1. Introduction

As the Earth's third pole, the Tibetan Plateau (TP) plays a critical role in influencing regional and global climate. The huge heat source in the mid-troposphere provided by the TP is perceived as an important factor contributing to the formation and variation of the Asian summer monsoon (Chen et al., 1985; Ye and Wu, 1998; Wu et al., 2012). Surface sensible heat (SH) flux is a major component of the heat source, and it plays a considerable role in modulating large scale atmospheric circulation and the summer monsoon precipitation patterns (Yanai et al., 1992; Zhao and Chen, 2000; Duan et al., 2013, 2017; Wang et al., 2014). So, many studies have attempted to estimate the spatiotemporal changes of SH flux over the TP using meteorological data (Duan and Wu, 2008; Duan et al., 2011; Guo et al., 2011; Yang et al., 2011), reanalysis data (Zhu et al., 2011; Shi and Liang, 2014; Xie et al., 2019), remote sensing products (Ma et al., 2011, 2012) or model simulations (Ma and Ma, 2016; Wang and Ma, 2019) these years.

Duan and Wu (2008) calculated the SH flux on the TP using data from meteorological stations and satellites for 1980-2003, and they found that the SH flux on the TP exhibited large diurnal range but much weaker annual range. The SH flux showed a significant decreasing trend since the mid-1980s to the beginning of the 21st century, and the subdued surface wind speed contributed most to the decreasing trend. Further, Duan et al. (2011) reexamined the trend in the SH flux during 1980-2008, and confirmed the weakening trend. They found that the trend was induced mainly by a reduction in surface wind speed, despite a sharp increase in the ground-air temperature difference in 2004-2008. They also considered it as a primarily response to the spatial nonuniformity of large-scale warming over the East Asian continent. Yang et al. (2011) investigated the differences between different methods for estimating trends in the SH flux on the TP using meteorological station data for the period 1984-2006. The results showed that different schemes produce different trends, and they claimed that SH flux on the TP weakened by 2% per decade using a new method developed by them. They claimed that the decrease in wind speed and the

increase in ground-air temperature difference may moderate the trend of the heat transfer coefficient, which in turn may influence the trend in SH flux. Wang and Ma (2019) performed several simulation experiments on the TP using the Noah-MP land surface model. The results show that the SH flux is very sensitive to the z0h parameterization scheme. Their results also supported the weakening trends from mid-1980s.

However, the weakening trend did not continue in the past decade (Zhu et al., 2017; Zhang et al., 2018; Chen et al., 2019). Zhang et al. (2018) calculated the SH flux over the TP using the meteorological station data from 1970 to 2015, and the temporal characteristics of SH flux were analyzed. They pointed out that there was an increasing trend in SH flux during 2001-2015. Chen et al. (2019) investigated the spatiotemporal variability in SH over the TP from 1980 to 2015 using data from meteorological station and reanalysis products. They also confirmed the increasing trend after the decreasing trend, and declared that the declines in SH prior to 2000 resulted from changes in wind speeds, and the subsequent recovery is attributable to increases in both wind speeds and air-surface temperature gradients.

Most of the previous studies estimated the SH flux on the TP using reanalysis datasets or meteorological station data by bulk transfer algorithms. There are many uncertainties in estimating the SH flux on the TP using data from unevenly distributed meteorological stations and diverse reanalysis datasets. The decadal trends of the SH flux, especially when and how the trends changed still remain controversial. This study will present high resolution simulations of the SH flux during 1985-2015 using Noah-MP land surface model. The climatic features of SH flux on the TP and the possible causes of the trends in the 31-yr simulation will be analyzed. In the next section, observations and the experimental design will be described.

# 2. Data And Methodology

Over the past a few decades, the TP experienced evident climate changes, and it amplified environmental changes to global scale as well. To mitigate the scarcity of observational data and to improve our understanding of land-atmosphere system, several field observational stations have already been established since the 1970s. In this study, the SH flux datasets used were collected from the eddy covariance (EC) systems at 3 observation stations. The QOMS station is situated at the bottom of the lower Rongbuk Valley, to the north of Mt. Everest. The EC system was installed at a height of 3.25m above ground level. The Nam CO station is located on the southeast shore of the Nam Co Lake in the central TP. The EC system was installed at a height of 3.06m above ground level. The Ali station was built in a flat and open mountain valley in the northwestern TP, where the Indian monsoon and westerly wind interact intensively. The EC system was installed at a height of 2.75m above ground level. Figure 1 shows the locations of the stations, and Table 1 gives the observation period and the information of the EC instruments. The details of the stations and data have been introduced in several previous studies (Li et al., 2015; Ma et al., 2020). All the datasets were quality-controlled using the TK3 software (Mauder and Foken, 2011).

Table 1
Details of the 3 stations and observing periods.

| Station | Location | Land use | Sonic anemometer | Period (yr) |
|---|---|---|---|---|
| QOMS | 28.36°N, 86.95°E | Bare soil | CSAT3 | 2008, 2010, 2011, 2012 |
| Nam Co | 20.77°N, 90.98°E | Alpine steppe | CSAT3 | 2008, 2009, 2011, 2012 |
| Ali | 33.39°N, 79.70°E | Desert | CSAT3 | 2011,2012,2013 |

We used the Noah-MP land surface model for the simulation, which is developed from the Noah land surface model (version 3.0) with multiple parameterization options (Niu et al., 2011; Yang et al., 2011). This model is suitable for the land surface process simulation over the TP according to previous studies (Gao et al., 2016; Zhang et al., 2020). In our simulation, the SIMGM runoff scheme, the Noah β-factor scheme, and the BATS snow surface albedo scheme were selected.

The thermal roughness length ($z_{0h}$) is a height at which the extrapolated air temperature is identical to the surface skin temperature, and cannot be measured directly. The parameterization of $z_{0h}$ is crucial for directly using surface temperature to calculate turbulent fluxes. A simple approach to specify $z_{0h}$ for the model grid cells is to assume that $z_{0h}$ is a fixed fraction of $z_{0m}$. Zeng and Dickinson (2008) proposed a Reynolds number-dependent formulation:

$$z_{0h} = z_{0m} \times \exp(-1.0k\alpha CRe_*^{0.45}) \quad (1)$$

where $C$ is an empirical constant, which modulates how strongly the $z_{0h}/z_{0m}$ ratio depends on roughness Reynolds number $Re_*$. $\alpha = 0.52$, $\beta = 7.2$, $C = 0.075$, $Pr = 0.71$. According to the result of Wang and Ma (2019), this thermal roughness length scheme made the best estimation of monthly mean SH flux in terms of squared correlation coefficients. We selected this scheme in the following simulation experiments.

The simulation experiments were conducted at a spatial resolution of 0.1° using CMFD data (He et al., 2020) as the atmospheric forcing dataset. This dataset was produced by merging a variety of data sources. The spin-up was performed with a two-stage procedure: (1) iteratively run the model for 100 years (using the forcing data of 1979) and (2) simulate another 1 year period from 1 January 1980 to 31 December 1980. Following the spin-up procedure, all experiments simulated the period from 1 January 1981 to 31 December 2015. The simulation results of 1985-2015 were calculated and analyzed in this study.

To assess the simulations, statistical methods such as correlation coefficient, squared correlation coefficient ($R^2$), linear least-squares regression and Mann-Kendall trend test are used.

# 3. Results

## 3.1. Assessment of the simulation

Before the analysis of the trends in simulated SH flux, a validation was performed using the in situ observation data at the 3 stations. The linear regression method was applied here. Figure 2a show the comparison between simulated and observed monthly mean SH fluxes at the QOMS station for 4 years (2008, 2010-2012). The blue dots represent the monthly mean values, and the blue line is the best-flit line. The squared correlation coefficient ($R^2$) is 0.719, with a root-mean-square error (RMSE) of 11.126 $Wm^{-2}$. Overall, the simulated SH fluxes were higher than the corresponding observations. At the Nam CO station, there were many missing observations in the dataset during the observing period (2008-2009, 2011-2012). So, the mean values of SH flux in 5 months were not obtained. The squared correlation coefficient is 0.678, with a RMSE of 10.216 $Wm^{-2}$. The simulated mean SH fluxes fit well with the observations for most of the 43 months (Figure 2b). Figure 2c show the comparison between simulated and observed monthly mean SH fluxes at the Ali station for 3 years (2011-2013). As there are many missing values in the dataset, only 27 monthly mean values are obtained here. The squared correlation coefficient is 0.682, with a bigger RMSE comparing with the former two.

## 3.2. Simulated sensible heat flux and its trends

From the analysis in the section above, the simulation of SH flux was overall suitable. The spatial distribution of the simulated 31-yr mean SH flux is shown in Figure 3a. According to previous studies (Duan and Wu, 2008; Yang et al., 2011), we divided the TP for 3 climate zones: dry western TP (west of 85°E), transitional central TP (85°E-95°E), and wet eastern TP (east of 95°E). The eastern TP received much lower 31-yr mean SH fluxes than the central and western TP, with values of 35.1 $Wm^{-2}$, 44.5 $Wm^{-2}$, and 48.1 $Wm^{-2}$, respectively. The areas with mean SH fluxes greater than 50 $Wm^{-2}$ were mainly in the southwestern TP region.

Figure 3b shows the variations in the annual mean SH flux during 1985-2015. Areas with a large standard deviation (STD) indicate large inter-annual variations of the SH flux, and vice versa. Large STD values were mainly observed over the central and western TP, while small STD values were mainly observed over the areas east of 92°E. This means that the central and western TP had larger inter-annual variations of the SH flux than the eastern TP.

We also analyzed the trends of the SH flux over the whole TP. Figure 4 shows the linear trends for the western, central, eastern and entire TP. The SH flux among the three sub-regions and over the entire TP exhibited significant decreasing trends since the mid-1980s, as was also reported by previous studies. These decreasing trends were more obvious on the western and central TP than on the eastern TP. However, all the regions showed an increasing trend since the beginning of 21st century. In 2002, the western, central, and entire TP got the lowest mean SH fluxes. From then on, the western and central TP began an increasing trend, while the eastern TP showed an increasing trend from about 2005. On the whole, the decreasing trend was about 0.39 $W/m^2$ per yr, while the increasing trend was 0.85 $W/m^2$ per yr.

# 3.3. Causes for the trends

The bulk transfer coefficient method is typically used to calculate the surface SH flux. Given the wind speed and ground-air temperature difference, SH flux can be calculated by

$$SH = \rho c_p C_H U (T_s - T_a) \quad (2)$$

where $\rho$ is air density, $c_p$ is the specific heat at a constant pressure, $u$ is the wind speed at a reference level, $Ts$ is ground temperature, $Ta$ is air temperature at the reference level, and $C_H$ is the heat transfer coefficient. $C_H$ is not a given constant value, and its value of $C_H$ can be obtained by different parameterization schemes (Yang et al., 2008; Chen et al., 2009).

So, the $Ts-Ta$, wind speed, and $C_H$ were analyzed to find the main causes of the increasing and decreasing trends. Figure 5 shows the simulated mean $Ts-Ta$ and its standard deviation on the TP during 1985-2015. The western and central TP had larger mean values of $Ts-Ta$ than the eastern TP. The distribution of annual mean values was very close to that of annual mean SH flux. The central and western and TP also had larger inter-annual variations than the eastern TP.

The trends of mean $Ts-Ta$ were shown in Figure 6 for the western, central, eastern and entire TP. There was an obvious decreasing trend from mid-1980s to the beginning of the 21st century on the western TP (Figure 6a). Then, it turned sharply upward. This phenomenon also existed on the central TP (Figure 6b). Figure 6c shows the annual mean values of $Ts-Ta$ and its trends in the eastern TP region. The values of $Ts-Ta$ were smaller than those of the western and central TP. Meanwhile, both the decreasing trend and increasing trend were not as significant as those of the western and central TP. The TP-average trends are shown in Figure 6d. Both the decreasing trend and increasing trend were significant, and this is similar to the trends of annual mean SH flux shown in Figure 4d. The correlation coefficient between annual mean SH flux and $Ts$-$Ta$ was 0.745.

Figure 7 shows the wind speed (10m above the ground) and its standard deviation on the TP during 1985-2015. The wind speed data was derived from the atmospheric forcing data (CMFD). The central and western TP got larger wind than the eastern TP during the 31yrs. The inter-annual variation values on the western TP also larger than those on the eastern TP. The annual variation of wind speed is shown in Figure 8. The values of annual mean wind speed in all the three sub-regions declined from mid-1985, and then increased from about 1998. However, these changes were not very clear, especially in the eastern TP. Overall, the wind speed over the TP decreased from 1985 to 1998, and then turned upwards after 1998 (Figure 8d). The changes of wind speed contributed a lot to the trends of SH flux before 1998.

Nevertheless, the heat transfer coefficient $C_H$ was also analyzed to show the annual variations. However, there were no clear trends in all the three sub-regions. The changes of surface wind speed and the ground-air temperature difference were the two major factors attributed to the changes of the SH flux, as reported in previous studies (Duan et al., 2011; Yang et al., 2011; Chen et al., 2019). From the analysis

above, it is found that surface wind speed began the increasing trend prior to 1998, while ground-air temperature difference turned sharply upward after 2002. So, the ground-air temperature difference contributed more than wind speed to the trends in SH flux during 1998-2002.

# 4. Conclusions And Discussion

We analyzed the climatic features of the SH flux simulated for 31 yrs (1985-2015). The parameterization scheme for thermal roughness length in the Noah-MP model was modified before the simulations. The major findings from our study are as follows:

(1) The western and central TP witnessed much larger 31-yr mean SH fluxes than the eastern TP. Meanwhile, the inter-annual variations of SH fluxes on the central and western TP were larger than that on the eastern TP. The decreasing trend in SH flux on the TP from mid-1980s to the beginning of the 21st century, as also reported by previous studies, was confirmed. The western and central TP began an increasing trend from about 2002. The trend shift on the eastern TP began later than the other two. On the whole, the increasing trend began from about 2002.

(2) Overall, there was a close relationship between the changes of mean $Ts-Ta$ and the trends in the SH flux. The changes of mean $Ts-Ta$ were the main cause of the decreasing and increasing trends in SH flux on the TP. Meanwhile, the changes of wind speed after 1998 was not as important as $Ts-Ta$ in terms of modulating the trends of SH flux. There were no clear trends in heat transfer coefficient $C_H$.

It should be point out that, the wind speed derived from reanalysis product was at 10m height above the ground. Wind speed at the height of 10m was widely used to calculated $C_H$ and SH flux based on the bulk transfer coefficient method. This may result in larger SH fluxes than the EC system. From the analysis of the simulations, the SH flux on the TP showed a decreasing trend in SH flux from mid-1980s, but an increasing trend since about 2002. The changes of mean $Ts-Ta$ were attributed as the main cause of the decreasing and increasing trends in SH flux on the TP. Both the changes of $Ts-Ta$ and wind speed contributed a lot to the trends of SH flux before 1998. The inconformity of changes in surface wind speed and ground-air temperature difference may result in disagreements in the cause for the trends in the SH flux on the TP in some previous studies.

# Declarations

**Funding:** This work was supported by the Second Tibetan Plateau Scientific Expedition and Research (STEP) program [grant no. 2019QZKK0103], and the National Natural Science Foundation of China [grant no. 42075156 and 91837208].

**Competing Interests:** The authors declare there are not competing interests.

**Ethics approval:** Not applicable.

**Consent to participate:** All authors agree consent to participate in this study.

**Consent for publication:** All authors have read and approved the final manuscript.

**Data availability:** The datasets generated and analyzed during the current study are not publicly available, but are available from the corresponding author on reasonable request.

**Code availability:** The software codes used during the current study are available from the corresponding author on reasonable request.

**Authors' contributions:** All authors contributed to the study conception and design. Data collection and analysis were performed by Shuzhou Wang, Yaoming Ma, and Yuxin Liu. The first draft of the manuscript was written by Shuzhou Wang and Yuxin Liu.

# References

Chen F, Zhang Y (2009) On the coupling strength between the land surface and the atmosphere: From viewpoint of surface exchange coefficients. Geophys Res Letters 36: L10404, doi: 10.1029/2009GL037980

Chen L, Pryor SC, Wang H, et al. (2019) Distribution and variation of the surface sensible heat flux over the central and eastern Tibetan Plateau: Comparison on of station observations and multireanalysis products. J. Geophys Res Atmos 124: 6191- 6206

Chen LX Reiter E, Feng Z (1985) The atmospheric heat source over the Tibetan Plateau: May-August 1979. Mon Wea Rev 113: 1771–1790

Duan AM, Wu GX (2008) Weakening trend in the atmospheric heat source over the Tibetan Plateau during recent decades. Part I: Observations. J Clim 21: 3149–3164

Duan AM, Li F, Wang MR, et al. (2011) Persistent weakening trend in the spring sensible heat source over the Tibetan Plateau and its impact on the Asian summer monsoon. J Clim 24: 5671–5682

Duan AM, Wang MR, Lei YH, et al (2013) Trends in summer rainfall over China associated with the Tibetan Plateau sensible heat source during 1980–2008. J Clim 26: 261–275

Duan AM, Sun R, He J. (2017) Impact of surface sensible heating over the Tibetan Plateau on the western Pacific subtropical high: A land–air–sea interaction perspective. Adv Atmos Sci 34: 157–168

Gao YH, Li K, Chen F, et al. (2015) Assessing and improving Noah-MP land model simulations for the central Tibetan Plateau. J Geophys Res Atmos120: 9258–9278

Guo XF, Yang K, and Chen YY, (2011) Weakening sensible heat source over the Tibetan Plateau revisited: effects of the land-atmosphere thermal coupling. Theor Appl Climatol 104: 1–12

He J, Yang K, Tang WJ, et al. (2020) The first high-resolution meteorological forcing dataset for land process studies over China. Scientific Data 7: 25

Li MS, Babel W, Chen XL et al (2015) A 3-year dataset of sensible and latent heat fluxes from the Tibetan Plateau, derived using eddy covariance measurements. Theor Appl Climatol 122: 457–469

Ma WQ, Ma YM (2016) Modeling the influence of land surface flux on the regional climate of the Tibetan Plateau. Theor Appl Climatol 125: 45–52

Ma YM, Zhong L, Wang BB, et al. (2011) Determination of land surface heat fluxes over heterogeneous landscape of the Tibetan Plateau by using the MODIS and in situ data. Atmos Chem Phys 1: 10461–10469

Ma YM, Wang BB, Zhong L, et al. (2012) The regional surface heating field over the heterogeneous andscape of the Tibetan Plateau using MODIS and in-situ data. Adv Atmos Sci 29: 47-53

Ma YM, Hu ZY, Xie ZP, et al. (2020) A long-term (2005-2016) dataset of hourly integrated land-atmosphere interaction observations on the Tibetan Plateau. Earth Sys Sci Data 12: 2937–2957

Mauder M, Foken T (2011) Documentation and instruction manual of the eddy covariance software package TK3, Work Report University of Bayreuth

Niu GY, Yang ZL, Mitchell KE et al (2011) The community No ah land surface mode l with multiparameterization options (Noah-MP): 1. Model description and evaluation with local-scale measurements. J Geophys Res 16: D12109, doi:10.1029/2010JD015139

Shi Q, Liang S (2014) Surface-sensible and latent heat fuxes over the Tibetan Plateau from ground measurements, reanalysis, and satellite data. Atmos Chem Phys 14: 5659–5677

Wang SZ, Ma YM (2019) On the simulation of sensible heat flux over the Tibetan Plateau using different thermal roughness length parameterization schemes. Theor Appl Climatol 137: 1883–1893

Wang ZQ, Duan AM, Wu GX (2014) Time-lagged impact of spring sensible heat over the Tibetan Plateau on the summer rainfall anomaly in East China: case studies using the WRF model. Climate Dynamics 42: 2885–2898

Wu GX, Liu YM, He B (2012) Thermal controls on the Asian summer monsoon. Sci Rep 2: doi: 10.1038/srep00404

Xie J, Yu Y, Li JL et al. (2019) Comparison of surface sensible and latent heat fluxes over the Tibetan Plateau from reanalysis and observations. Meteorol Atmos Phys 131: 567–584

Yanai M, Li CF, Song ZS (1992) Seasonal heating of the Tibetan Plateau and its effects on the evolution of the Asian summer monsoon. J Meteorol Soc JP 70: 319–351

Yang K, Koike T, Ishikawa H, et al (2008) Turbulent flux transfer over bare-soil surfaces: characteristics and parameterization. J Appl Meteorol Climatol 47: 276–290

Yang K, Guo XF, Wu BY (2011) Recent trends in surface sensible heat flux on the Tibetan Plateau. Sci China Ser D 54: 19–28

Yang ZL, Nlu GY, Mitchell KE et al (2011) The community Noah land surface model with multiple parameterization options (Noah-MP): 2. Evaluation over global river basins. J Geophys Res 116: D12110, doi:10.1029/2010JD015140

Ye DZ, Wu GX (1998) The role of the heat source of the Tibetan Plateau in the general circulation. Meteorol Atmos Phys 67: 181–198

Zeng XB, Dickinson RE (1998) Effect of surface sublayer on surface skin temperature and fluxes. J Clim 11: 537–550

Zhang C, Tian RX, Mao HL, et al. (2018) Temporal and spatial variation of surface sensitive heat fluxes over the middle and eastern Tibetan Plateau. Adv. Clim. Change Res. 14: 127-136.

Zhang G, Chen F, Chen YL, et al. (2020) Evaluation of Noah-MP Land-Model uncertainties over sparsely vegetated sites on the Tibet Plateau. Atmosphere 11: 458

Zhao P, Chen LX (2000) Study on climatic features of surface turbulent heat exchange coefficients and surface thermal sources over the Qinghai-Xizang (Tibetan) Plateau. Acta Meteor Sinica 14: 13–29

Zhu LH, Huang G, Fan GZ, et al. (2017) Evolution of surface sensible heat over the Tibetan Plateau under the recent global warming hiatus. Adv Atmos Sci 34: 1249–1262

Zhu XY, Liu YM, Wu GX (2012) An assessment of summer sensible heat flux on the Tibetan Plateau from eight data sets. Sci China Earth Sci 55: 779–786

# Figures

### Figure 1

The location of the 3 stations (black dots) on the Tibetan Plateau.

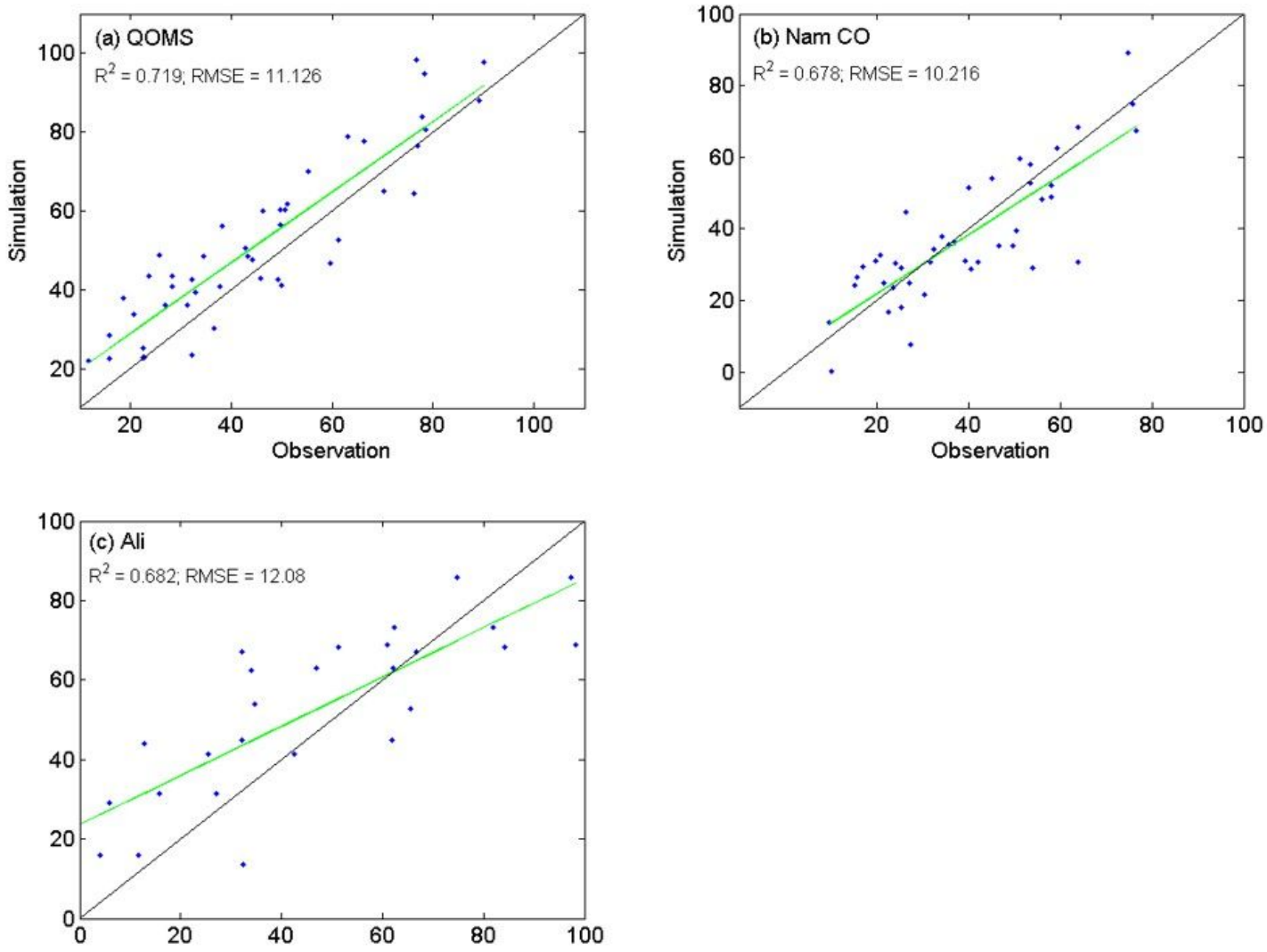


## Figure 2

Comparison of between simulated and observed monthly mean SH fluxes ($Wm^{-2}$) at the QOMS station (a), Nam CO station (b), and Ali station (c). The green line is the best-fit line in each plot.

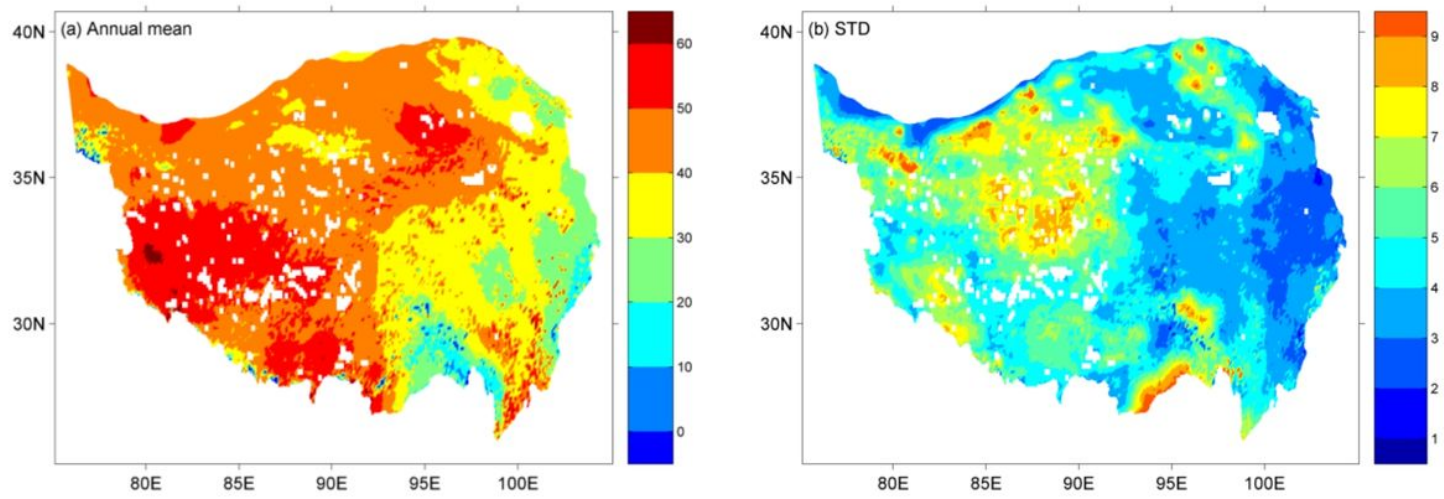


## Figure 3

Simulated (a) mean SH flux ($Wm^{-2}$) and the standard deviation (b) of SH flux ($Wm^{-2}$) on the TP during 1985-2015.

## Figure 4

Trends in annual mean SH flux ($Wm^{-2}$) for the western (a), central (b), eastern(c), and entire TP (d) during 1985-2015. All of the trends are derived from linear least-squares regressions and significant at the 95% confidence level using the Mann-Kendall trend test.

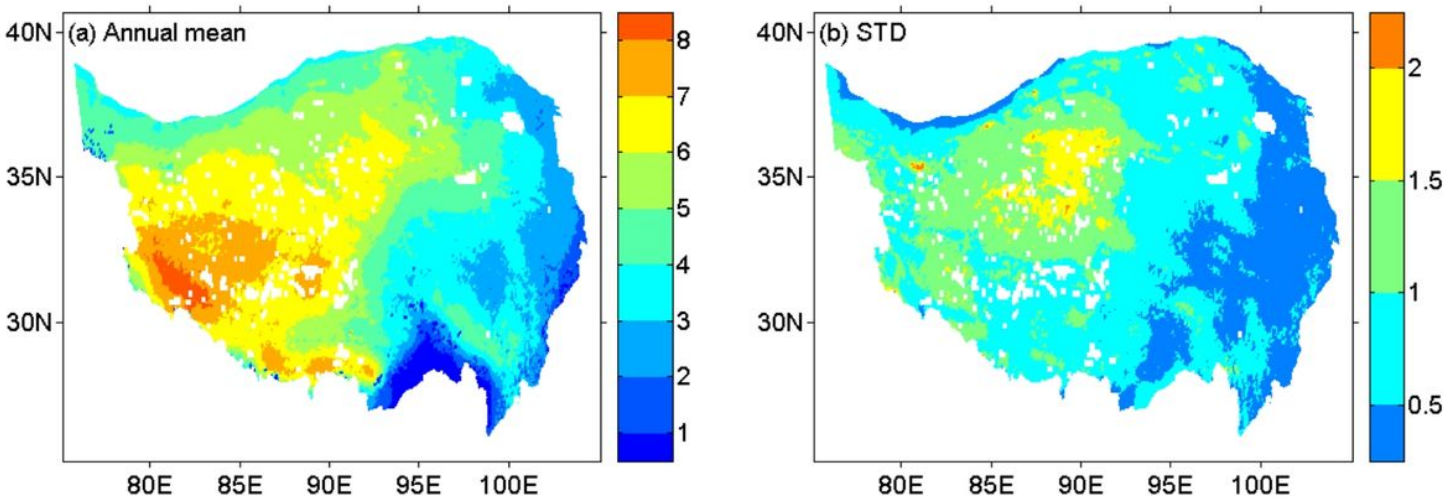


## Figure 5

Simulated (a) mean Ts-Ta (K) and the standard deviation of Ts-Ta (K) on the TP during 1985-2015.

## Figure 6

Trends in annual Ts-Ta (K) for the western (a), central (b), eastern (c), and entire TP (d) during 1985-2015. All of the trends are derived from linear least-squares regressions and significant at the 95% confidence level using the Mann-Kendall trend test.

## Figure 7

Simulated (a) annual mean wind speed (m/s) at 10m above the ground and the standard deviation (b) of wind speed (m/s) on the TP during 1985-2015.

## Figure 8

Annual mean wind speed (m/s) for the western (a), central (b), eastern (c), and entire TP (d) during 1985-2015. All of the trends are derived from linear least-squares regressions and significant at the 95% confidence level using the Mann-Kendall trend test.